HHS Public Access

Author manuscript

J Biomed Mater Res B Appl Biomater. Author manuscript; available in PMC 2015 September 04.

Published in final edited form as:

J Biomed Mater Res B Appl Biomater. 2014 October ; 102(7): 1363–1374. doi:10.1002/jbm.b.33115.

Corrosion resistance improvement for 316L stainless steel coronary artery stents by trimethylsilane plasma nanocoatings

John Eric Jones[1], **Meng Chen**[2], and **Qingsong Yu**[1]

[1]Center for Surface Science and Plasma Technology, Department of Mechanical & Aerospace Engineering, University of Missouri, Columbia, Missouri 65211

[2]Nanova, Inc., Columbia, Missouri 65211

Abstract

To improve their corrosion resistance and thus long-term biocompatibility, 316L stainless steel coronary artery stents were coated with trimethylsilane (TMS) plasma coatings of 20–25 nm in thickness. Both direct current (DC) and radio-frequency (RF) glow discharges were utilized for TMS plasma coatings and additional NH_3/O_2 plasma treatment to tailor the surface properties. X-ray photoelectron spectroscopy (XPS) was used to characterize the coating surface chemistry. It was found that both DC and RF TMS plasma coatings had Si- and C-rich composition, and the O- and N-contents on the surfaces were substantially increased after NH_3/O_2 plasma treatment. Surface contact angle measurements showed that DC TMS plasma nanocoating with NH_3/O_2 plasma treatment generated very hydrophilic surface. The corrosion resistance of TMS plasma coated stents was evaluated through potentiodynamic polarization and electro-chemical impedance spectroscopy (EIS) techniques. The potentiodynamic polarization demonstrated that the TMS plasma coated stents imparted higher corrosion potential and pitting potential, as well as lower corrosion current densities as compared with uncoated controls. The surface morphology of stents before and after potentiodynamic polarization testing was analyzed with scanning electron microscopy, which indicated less corrosion on coated stents than uncoated controls. It was also noted that, from EIS data, the hydrophobic TMS plasma nanocoatings showed stable impedance modulus at 0.1 Hz after 21 day immersion in an electrolyte solution. These results suggest improved corrosion resistance of the 316L stainless steel stents by TMS plasma nanocoatings and great promise in reducing and blocking metallic ions releasing into the bloodstream.

Keywords

corrosion; stainless steel; stents; coatings; electron microscopy

INTRODUCTION

Since their introduction in the mid-1980s, 316L stainless steel coronary artery stents have been a valuable asset in treating occluded arteries.[1–4] Each year, nearly 1.4 million stents are implanted worldwide.[5,6] Unfortunately, in-stent restenosis occurs within 20–40% of stent

Correspondence to: M. Chen; mengchen2002slc@yahoo.com or Q. S. Yu; yuq@missouri.edu.

recipients.[7] Restenosis occurs due to inflammation of the tissues in contact with the stent. Smooth muscle cells, which are normally present within the vasculature, proliferate extensively and thus eventually closing the stented vessel.[8–10] Such closure requires invasive corrective action that could ultimately result in arterial bypass.[11]

Stent corrosion released particles, primarily nickel, have been implicated as agents of restenosis.[10] The corrosion process within the body is due to the presence of proteins and shearing stresses along the stent surface.[12,13] In addition to inflammation, nickel particles have been implicated as potentially carcinogenic.[13] The corrosion process starts within days of implantation and can potentially lead to loss of arterial structural integrity.[14]

To date, tremendous efforts have been made to improve the corrosion resistance of implant metals by using various surface treatment techniques.[15–17] Ion implantation and laser treatment are effective methods to enhance the corrosion resistance of metallic materials. However, it is very expensive and difficult to treat a complex shape implant such as vascular stents or staples by using these two methods.[15,16] Some research works have focused on applying coatings to stents so as to improve their hemocompatibility. Surface coatings with hard and rigid bioceramics (TiN, TiCN, Al_2O_3, SiC, BN, and Si_3N_4) fail in stenting applications due to the cracking of these coatings because of the expansion during stent dilatation.[17] Other coatings include polymers,[18,19] gold,[20,21] and diamond and graphite[22,23] have also been explored. Unfortunately, while inhibiting corrosion of the base stent, the coatings themselves can induce an inflamma-tory response. Alternatively, amorphous silicon carbide (a-SiC:H) coatings have been investigated for improving stent biocompatibility. It was found that such silicon carbide coatings could block electron transfer reactions between the blood protein fibrinogen and the underlying metallic stent and thus halt thrombus formation.[24–26] Pre-clinical studies have shown that surface passivation of stents by a-SiC:H coating could reduce thrombogenecity and possibly improve the biocompatibility of stent surfaces. Clinical trials have generally shown low rates of stent thrombosis in patients with stenotic lesions.[27]

It is known that low temperature plasma techniques can be used to deposit silicon carbide-like plasma nanocoatings with well-tailored surface chemistry, which could be advantageous for coronary artery stent applications. In comparison with bioceramic coatings, plasma nanocoatings with controllable physical properties, which include hard inorganic oxide, carbide, or nitride to various soft plasma coatings, can be easily produced by adjusting the plasma chemistry and plasma conditions. A variety of desired surface properties such as biocompatibility, hemo-compatibility, and surface energy are achievable by controlled plasma chemistry. With regard to biomaterials engineering, the typical advantages offered by plasma coating deposition techniques include: (i) Plasma processes are usually reliable, reproducible, and applicable to different sample geometry with complex shapes; (ii) Plasma treatment without coating deposition can result in surface cleaning, and changes of surface characteristics, e.g., chemical, physical, biological; (iii) Plasma coating deposition creates nanoscale coatings, which are conformal, free of voids, and chemically inert, possessing excellent barrier property and superior adhesion to various substrates; (iv) Plasma processing provides a sterile surface and is relatively inexpensive, easily operated, dry, and rapid.[28] In addition, plasma nanocoatings are generally formed in an extremely tight and

three-dimensional network, which is more like a low-permeability sieve with excellent barrier properties for transport of various ionic species, and consequently significantly impede corrosion.[26] It is expected that the excellent barrier property of plasma coatings can improve the corrosion resistance and thus reduce the corrosion induced ion release and enhance the biocompatibility of implantable devices such as coronary artery stents.

In this study, trimethylsilane (TMS) plasma nanocoatings were deposited onto coronary artery stents and their corrosion resistance was investigated using different methods. Both direct current (DC) and radio frequency (RF) power sources were utilized to ignite glow discharge plasmas. RF glow discharges have been more extensively used in plasma coating deposition processes because of their well-recognized stability, yet DC glow discharges may be more advantageous for the deposition of plasma nanocoatings in term of adhesion to metallic substrates. Additional surface treatments of TMS plasma coatings using ammonia and oxygen based glow discharges were used to tailor the coating surface wettability. The corrosion resistance and barrier properties of the TMS plasma nanocoatings were investigated by electrochemical techniques including potentiodynamic polarization and electrochemical impedance spectroscopy (EIS). These studies will provide vital information on the corrosion behavior of the plasma coated stents implanted in coronary arteries of patients as to determine whether they hold promise for ultimate clinical application.

EXPERIMENTS

Stent coatings with DC- and RF-based glow discharges

316L stainless steel coronary artery stents of 1.6 mm × 12 mm (diameter × length) were purchased from STI Laser Industries (Or Akiva, Israel). Before use, the stents were first sonicated in isopropanol for 30 min and then further sonicated in distilled water for 30 min to remove residual isopropanol. Anhydrous ammonia (purity > 99.99%) was provided by Air Liquide (Plumsteadville, PA). Oxygen (purity > 99.6%) was purchased from Airgas (Columbia, MO). TMS (purity > 97%) was supplied by Gelest, Inc. (Morrisville, PA).

DC glow discharges were created inside an 80-L bell-jar reactor. Stents were attached to a metal holder positioned between two titanium electrodes in parallel. The square titanium electrodes had sides of length 18.2 cm. For all DC treatments, the stent holder acted as the cathode whereas the two outer titanium electrodes served as the electrically grounded anodes. An oxygen plasma was used to remove organic contaminants on the sample surfaces and provide a controllable fresh surface for the subsequent plasma coating deposition. The reactor was sealed and evacuated to a base pressure of 1 mTorr using a pump group consisting of mechanical and booster pumps connected in series. Oxygen was then introduced to the reactor at a flow rate of 1 sccm (standard cubic centimeters per minute) using an MKS mass flow controller (MKS Instruments, Andover, MA) and an MKS 247C readout to set the flow rate. The pressure inside the plasma reactor was allowed to stabilize at 50 mTorr using an MKS pressure controller. The oxygen was then excited with the DC power supply at 20 W in order to form the plasma. The treatment time was 2 min. Following surface cleaning, the reactor was evacuated to the base pressure of 1 mTorr and TMS was introduced to the reactor at 1 sccm. The reactor pressure was allowed to reach 50 mTorr, and the TMS was excited by the DC power supply at 30 W for 15 s.

For samples requiring surface modification of the plasma coating, the reactor was evacuated to a pressure of 1 mTorr and the treatment gases were then introduced. The gas composition used for the surface modified samples was a mixture of NH_3 plus O_2 at a ratio of 2:1. The pressure was allowed to equilibrate at 50 mTorr, and the plasma was induced by applying 5 W DC power, and the treatment lasted 2 min for the surface modification step.

The gas mixtures used to sustain the DC glow discharge (DCGD) for surface treatments were also employed in the case of RF glow discharge (RFGD) generated by a 13.56 MHz RF power source (RFX-600, Advanced Energy Industries, Inc., Fort Collins, CO). In the arrangement for RF plasma surface treatment and coating deposition, the aluminum panel with the stainless steel coupons to be coated was placed between two active electrodes. The panel was maintained at a floating potential versus the electrodes. The oxygen plasma pretreatment step was carried out at a power of 20 W RF and a mass flow of 1 sccm for 2 min. Following the treatment, the samples were coated with the TMS plasma coating deposited at 30 W RF for 5 min. One of the RF plasma coated groups was further modified with NH_3/O_2 mixture plasma at 5 W RF for 2 min. All steps were carried out at a working pressure of 50 mTorr.

Surface wettability assessment of coated 316L stainless steel

To determine the effect of plasma treatment on the surface wettability, 316L stainless steel coupons of 10 mm × 10 mm × 1 mm (width × length × thickness) were treated under the same conditions as described above. Coupons were linked to the aluminum panel with silver paint. Surface contact angles were measured using a 1 μL droplet of distilled water deposited onto the substrate surface, and a computer-aided VCA 2500 XE Video Contact Angle System (AST Products, Inc., Billerica, MA). Surface wettability changes over time after plasma treatment were evaluated by taking surface contact angle measurements 1, 7, 14, and 21 days following removal of the coupons from the bell-jar reactor.

Surface chemistry analysis

X-ray photoelectron spectroscopy (XPS) was used to determine surface chemistry composition of coated stainless steel coupons. A Kratos AXIS 165 X-ray Photoelectron Spectrometer (Kratos Analytical Inc., Chestnut Ridge, NY) utilizing a monochromatic Al Kα X-ray (1486.6 eV) source operating at 150 W was utilized to characterize the coatings to a depth of about 10 nm. The X-ray source take-off angle was set at 90° relative to the coupon surface, and the spot size was 200 μm × 200 μm.

Determination of corrosion potentials and current densities of coated stents

After plasma coating, stainless steel stents were expanded from 1.6 mm to 3 mm in diameter using a dilatation balloon catheter to mimic the clinical situation in which a stent is delivered to a narrowed coronary artery and dilated to a size that matches the diameter of healthy artery to propopen the diseased blood vessel and restore normal blood flow. Those stents were attached to a borosilicate fixture. A stainless steel wire was then attached to the stent using a small droplet of silver paint. The free end of the wire was threaded through the holder. After the paint dried, the wire-stent contact area, the steel wire, and the bottom opening of the holder were covered with epoxy. The exposed stent surface area was 0.1563

cm^2, as provided by the stent supplier. After the epoxy set, the stent was placed inside the corrosion cell containing phosphate buffered saline (PBS) (8.0 g/L NaCl, 0.2 g/L KCl, 1.15 g/L $Na_2HPO_4 \cdot 7H_2O$, 0.2 g/L KH_2PO_4). The stents were kept submerged for 2 h prior to potentiodynamic polarization testing.

Potentiodynamic polarization testing was carried out with a Model 273A Potentiostat/Galvanostat (EG & G, Princeton Applied Research, Oak Ridge, TN) using the Power Suite software package. This testing technique is built on the concept that predictions of behavior of a stainless steel material in an environment can be made by forcing the material from its steady state corrosion rate at a constant voltage scan rate and by observing how the current responds as the voltage force is applied. A conventional three electrode arrangement was used with stainless steel stents as the working electrode, a saturated Ag/AgCl + 3.5*M* KCl electrode as the reference electrode, and a graphite rod of 0.6 cm in diameter as the counter electrode. The rest potential was monitored for 2 h prior to testing in PBS, which insured a stable open circuit potential. Potentiodynamic polarization curves were then generated starting at −200 mV relative to the open circuit potential and conducted until the corrosion current density reached 10^4 μA/cm^2. A scan rate of 20 mV/s was utilized during testing. Tafel extrapolation was used to determine E_{corr} (mV) and I_{corr} (μA/cm^2). Three replicate tests were performed for each group of specimens including DC plasma coated, RF plasma coated, and uncoated stents.

EIS measurements of coated stents

The three electrode cell used for potentiodynamic polarization testing was further utilized for EIS measurements, and PBS was used as the electrolyte. The applied AC signal was 10 mV RMS (Root Mean Square) in the frequency range of 10^{-1} Hz to 10^5 Hz. To monitor the stability of the coatings over time, EIS measurements were taken at 0.1 (2 h), 1, and 21 days following immersion in PBS. Bode and phase angle plots were collected for each specimen.

Scanning electron microscopy analysis of stent surface

A Quanta 600F Environmental scanning electron microscope (SEM) (FEI Company, Hillsboro, OR) was utilized to characterize the surface structure of stents before and after potentiodynamic polarization testing. An accelerating voltage of 10 kV was used for all measurements.

Statistical analysis

A total of $n = 3$ samples were used for all treatments. Students' *t*-tests were used to compare the corrosion potential and corrosion current densities of the uncoated stents with all coated stent groups. Differences were considered significant at $p < 0.05$.

RESULTS AND DISCUSSION

Figure 1 depicts the surface contact angle measurement results using 316L stainless steel wafers with and without plasma nanocoatings. The as-deposited TMS plasma coatings using both DC and RF power supplies (designated at DC-TMS and RF-TMS) was hydrophobic with contact angle ranging from about 105° to 110° at day 7 after plasma coating deposition

while those wafers modified with additional NH_3/O_2 plasma (designated as DC-TMS $+NH_3/O_2$ and RF-TMS$+NH_3/O_2$) showed higher surface energies indicated by smaller contact angle. The DC glow discharge plasma (DC-TMS$+NH_3/O_2$) was able to completely wet the plasma coating surfaces initially. After the 21 day aging period during which the samples were kept in a covered petri dish, the contact angle for the wafers modified with the DC glow discharge (DC-TMS$+NH_3/O_2$) increased due to hydrophobic recovery commonly seen with plasma modified surfaces; however, the contact angle did not rise above that of bare stainless steel, which is 42° in this case. The presence of hydrophilic moieties was verified with the XPS survey spectra as shown in Figure 2. Bare stainless steel coupons contained high quantities of C, O, Fe, Cr, and Si as well as trace amounts of N, Ni, and F (Table I). Adventitious carbon is due to the presence of organic materials on surface. The high concentration of oxygen could be attributed to the natural oxide layer formed on the metal surface. Plasma coating deposition results in higher concentrations of C and Si as expected from using TMS monomer [$(CH_3)_3$-SiH] that contains three C atoms and one Si atom in its molecular structure. The presence of oxygen on the TMS plasma coated surface was likely due to the surface oxidation when the coating material was exposed to air. A new N 1s peak appears for the surface modified DC and RF treatment groups, e.g. DC-TMS $+NH_3/O_2$ and RF-TMS$+NH_3/O_2$, as a result of the NH_3/O_2 plasma treatment. High resolution deconvolution of the C 1s peak in Figure 2 indicated the presence of C–C/C–H, C–O, and C=O bonding on the surface of the plasma coating. The composition of the TMS plasma coating layer in this study is similar to that of previous reseasrchers.[29]

Figure 3 shows the representative potentiodynamic polarization curves measured using 316L stainless steel stents with and without plasma nanocoatings. The potentio-dynamic polarization test can detect the relative susceptibility to localized corrosion on those stent samples. This test has been successfully used to evaluate the anti-corrosion characteristics of 316L stainless steel stents with deposited protective coatings.[30,31] From these scans, we can observe the corrosion potential (E_{corr}), pitting potential (E_{pitt}), and corrosion current density (I_{corr}). Table II depicts the values for E_{corr}, I_{corr}, and E_{pitt} for all specimens of five groups. All plasma coated stents showed significantly higher E_{corr} readings than bare stainless steel after the 2 h immersion time. In addition, the unmodified specimens with DC TMS coating only (identified as DC-TMS) resulting in hydrophobic surface showed substantially higher E_{corr} than the modified counter-parts with DC TMS coating and additional DC NH_3/O_2 treatment (identified as DC-TMS$+NH_3/O_2$) creating hydrophilic surface. This could be attributed to enhanced water penetration and salt intrusion of the plasma coating with hydrophilic surface in this DC plasma conditions. However this trend in E_{corr} change with DC plasma coated groups was not seen between RF-TMS and RF-TMS$+NH_3/O_2$ coated stents with the latter being unable to generate highly hydrophilic surface evidenced by the contact angle data shown in Figure 1. In fact, the E_{corr} value of RF-TMS$+NH_3/O_2$ coated stents appeared to be higher than RF-TMS coated counterparts, which could be attributed to the RF NH_3/O_2 treatment resulting in a denser top layer of crosslinking on the surface of RF-TMS coating through O and N incorporation on the surface as suggested by the XPS data (Table I). Plasma surface modification has been reported to cause crosslinking at the surface of polymeric materials for desired surface properties.[32–34] It is understood that DC-TMS coatings could have higher density or less porosity than their counterparts deposited in

RF plasma especially at the nanoscale coating thickness of 20–25 nm, because the specimens to be coated in DC plasma served as a cathode and ion bombardment to the cathode could help remove loosely bonded species from the growing coating surface. Whereas the specimens were kept floating in RF plasma condition, there was no strong ion bombardment effect expected on the growing coating surface. The corrosion rate is normally proportional to the corrosion current density I_{corr} measured in the polarization tests.[35] All the plasma coated stents had lower I_{corr} than bare 316L stents. Among the plasma coated groups, the I_{corr} of DC-TMS+NH_3/O_2 coated stents was higher than DC-TMS while RF-TMS+NH_3/O_2 had less I_{corr} than RF-TMS, which is in agreement with the E_{corr} data. Similar to the trend in E_{corr} and I_{corr}, all the four plasma coated groups showed significantly higher E_{pitt} than bare stainless steel stents, indicative of markedly improved corrosion resistance with plasma nanocoatings.

EIS was used to obtain further information on plasma coating barrier resistance during immersion periods of up to 21 days. EIS is a nondestructive and powerful testing method frequently used for assessing the barrier property and corrosion resistance performance of protective coatings on metals.[36–38] It was also utilized to evaluate the structure–property relationships of 316L stainless steel and how the fibrinogen adsorption was affected.[39] From EIS, Bode and phase angle plots can provide information on interfacial adhesion as well as electrolyte uptake by the coating. Figures 4–6 illustrate the Bode plots (impedance vs. frequency) and phase angle plots (phase angle vs. frequency) for the stents after 0.1, 1, and 21 day immersion in PBS respectively. Here 0.1 day indicates the initial run after 2 h immersion of the samples. The Bode plots in Figures 4(A), 5(A), and 6(A) show fluctuations over the 21-day period for all treatment groups and the uncoated control. This observation suggests degradation of the coatings over the testing period. Phase angle curves for the uncoated stents at the immersion times of 0.1 day, 1 day, and 21 days show a plateau from 10^{-1} to 10^{2} Hz with values around −80° , which confirms the that the natural oxide layer over the surface is capacitive and protective.[40,41] The phase angle plots for the DC-TMS plasma coating depict two plateaus that remain relatively stable for the immersion period of up to 21 days, indicating that the coating barrier property did not deteriorate noticeably over time. The plateau at higher frequency region (10^{3}–10^{4} Hz) is confirmation of the presence of plasma coating whereas the broader region near 10^{-1}–10° Hz indicates the oxide layer.[41] The DC-TMS+NH_3/O_2 coated stents showed a phase angle shape change over the immersion time from 0.1 day to 1 day and 21 days, in which the phase angle of the plateau at high frequency shifted from −40° to −47° or −50° with increasing immersion. This could be due to the hydrophilic surface created by additional NH_3/O_2 plasma treatment, thus resulting in more water uptake over immersion time. A phase shift at higher frequency region could also be attributed to a physical change in the coating due to the interaction of the ions present in the solution.[42] The phase angle plots of RF-TMS and RF-TMS+NH_3/O_2 coated stents appeared to be quite different than their counterparts of DC plasma coatings, indicative of different coating barrier property. This pattern suggested that there could be three time constants in the RF coated specimens: one in the high frequency range due to the coating, a second small one in the middle frequency range that can be ascribed to the response of processes occurring at the coating/substrate interface, and a third time constant in the low frequency range which is attributed to corrosion process.[43]

As shown in Figures 4(A), 5(A), and 6(A) for uncoated stents, the |Z| value at the frequency of 0.1 Hz was 78 kΩ, 89 kΩ, and 122 kΩ for the immersion time of 0.1 day, 1 day, and 21 days, respectively, which could indicate a passivation layer formed during the immersion period in this electrolyte, protecting the uncoated stent from further corrosion. The impedance at the low frequency of 0.1 Hz has been used as a key performance indicator for protective layer on metallic surface.[36,44] The higher the impedance value, the better the protective barrier property is. The increase in the impedance modulus for uncoated stents implying passivation layer formation was also reported by other reseachers.[45] From the Bode plots [Figures 4(A), 5(A), and 6(A)], we can see that the impedance modulus |Z| at 0.1 Hz for RF-TMS coated stents is higher than DC-TMS counterparts at day 21 after immersion even though there was obvious difference between them at day 0.1 or 1, which suggested that RF-TMS coating might provide better corrosion resistance than DC-TMS. It was also found that the impedance modulus |Z| at 0.1 Hz for RF-TMS+NH_3/O_2 coated stents was higher than that for DC-TMS+NH_3/O_2 coated ones, which appeared to be in agreement with the I_{corr} values of the two groups obtained by potentiodynamic polarization test (Table II). Likewise, Bode plots indicate substantially higher |Z| at 0.1 Hz for RF-TMS group over the testing period than bare metal. Coupled with the potentiodynamic polarization curves and data shown in Table II, the results suggest that both DC and RF plasma treatment groups can form a corrosion protection layer over bare metal stents.

Figures 7–11 depict the SEM images of stents before and after potentiodynamic polarization testing. All those stents including uncoated control and plasma coated were expanded using a balloon catheter prior to this corrosion testing. Non-tested bare stainless steel stents had smooth surface although very few debris was seen on the strut [Figure 7(A)]. All the plasma coated stents that did not go through corrosion test also showed smooth morphology [Figures 8(A), 9(A), 10(A), and 11(A)], and no coating cracking was present on the surface after expansion. Following potentiodynamic polarization testing, corrosion or coating cracking was observed on the stent surface [Figures 8(B), 9(B), 10(B), and 11(B)]. Pitting corrosion is extensive on the uncoated stent [Figure 7(B)]. No pitting was seen on the DC-TMS coated stent and the coating remained almost intact [Figure 8(B)] except slight coating cracking in very small area. There was no apparent pitting present on either DCTMS +NH_3/O_2 or RF-TMS coated stent surface as shown in Figures 9(B) and 10(B) respectively, but coating cracking was observed on both of them with likely more cracking in RF-TMS coating [Figure 10(B)]. Some sparse pits were seen on RF-TMS+NH_3/O_2 coated stent [Figure 11(B)], but much less than that on uncoated stent surface. These observations about pitting and coating cracking from SEM images seemed to correspond well to the results listed in Table II: high E_{pitt} and E_{corr} with corresponding low I_{corr} values for the coating groups indicate increased resistance to stent corrosion. To investigate the biological responses of the plasma coated stainless steel surfaces, thrombosis-resistance test, among many other *in vitro* cell culture tests, was also performed using leukocytes and platelets isolated from human blood. Assessing the attachment of platelets and leukocytes to plasma coated surfaces would help understand whether those plasma coatings improve thrombo-resistance when in contact with blood without causing infection. The thrombosis-resistance test results indicated the substantially less attachment of leukocytes and platelets to the plasma coated stainless steel wafers as compared to the uncoated controls (manuscript in

preparation). To ensure that the TMS-based plasma coating is nontoxic for medical implant application, cytotoxicity test was also performed using a protocol based on ISO 10993-5 guidance[46] and MTT assay. L-929 mouse fibroblast cells were seeded on to stainless steel wafers with and without TMS plasma coating and incubated for 24 h at 37° C in 5% CO_2. It was found that the TMS coating on stainless steel wafers had little to no effect on cell viability as compared to uncoated control (manuscript in preparation).

CONCLUSIONS

We have successfully deposited TMS plasma nanocoatings onto stainless steel stents. The plasma nanocoatings imparted higher E_{corr} and E_{pitt} values, and lower I_{corr} values as compared to the uncoated stents, which were in agreement with the corrosion characteristics observed in SEM images. Furthermore, EIS measurements illustrated long-term stability of hydrophobic plasma coatings (DC-TMS and RF-TMS) deposited on stents in electrolyte. These results from the corrosion studies suggest improved corrosion resistance of plasma coated stents. Thus, plasma nanocoatings may serve as a very promising barrier against the formation of corrosion particles that could result in restenosis of implanted stents.

ACKNOWLEDGMENTS

The authors would like to acknowledge the University of Missouri's Electron Microscopy Core Facilities for assistance in SEM imaging for this research. Authors also thank Brian Porter at Material Science Center, Missouri University of Science and Technology for his help in the XPS data analysis of the substrates.

Contract grant sponsor: National Heart, Lung, And Blood Institute of the National Institutes of Health; contract grant number: Award Number R44HL097485

REFERENCES

1. Schatz RA, Palmaz JC, Tio FO, Garcia F, Garcia O, Reuter SR. Balloon-expandable intracoronary stents in the adult dog. Circulation. 1987; 76:450–457. [PubMed: 2955956]
2. Schatz RA, Baim DS, Leon M, Ellis SG, Goldberg S, Hirshfeld JW, Cleman MW, Cabin HS, Walker C, Stagg J. Clinical experience with the Palmaz-Schatz coronary stent. Initial results of a multi-center study. Circulation. 1991; 83:148–161. [PubMed: 1984878]
3. Nakamura S, Colombo A, Gaglione A, Almagor Y, Goldberg SL, Maiello L, Finci L, Tobis JM. Intracoronary ultrasound observations during stent implantation. Circulation. 1994; 89:2026–2034. [PubMed: 8181126]
4. Haude M, Erbel R, Issa H, Meyer J. Quantitative analysis of elastic recoil after balloon angioplasty and after intracoronary implantation of balloon-expandable Palmaz-Schatz stents. J Am Coll Cardiol. 1993; 21:26–34. [PubMed: 8417068]
5. Mintz GS, Hoffmann R, Mehran R, Pichard AD, Kent KM, Satler LF, Popma JJ, Leon MB. In-stent restenosis: The Washington Hospital Center Experience. Am J Cardiol. 1998; 81:7E–13E. [PubMed: 9462597]
6. Schaefer O, Lohrmann C, Winterer J, Kotter E, Langer M. Endovascular treatment of superficial femoral artery occlusive disease with stents coated with diamond-like carbon. Clin Radiol. 2004; 59:1128–1131. [PubMed: 15556596]
7. Kastrati A, Mehilli J, von Beckerath N, Dibra A, Hausleiter J, Pache J, Schühlen H, Schmitt C, Dirschinger J, Schömig A. Sirolimus-eluting stent or paclitaxel-eluting stent vs balloon angioplasty for prevention of recurrences in patients with coronary instent restenosis, a randomized controlled trial. J Am Med Assoc. 2005; 293:165–171.

8. Huang Y, Venkatraman SS, Boey FYC, Umashankar PR, Mohanty M, Arumugam S. The short-term effect on restenosis and thrombosis of a cobalt-chromium stent eluting two drugs in a porcine coronary artery model. J Interv Cardiol. 2009; 22:466–478. [PubMed: 19627432]
9. Shedden L, Kennedy S, Wadsworth R, Connolly P. Towards a self-reporting coronary artery stent—Measuring neointimal growth associated with in-stent restenosis using electrical impedance techniques. Biosens Bioelectron. 2010; 26:661–666. [PubMed: 20667708]
10. Köster R, Vieluf D, Kiehn M, Sommerauer M, Kähler J, Baldus S, Meinertz T. Nick molybdenum contact allergies in patients with coronary in-stent restenosis. Lancet. 2000; 356:1895–1897. [PubMed: 11130387]
11. Heldman AW, Brinker JA. Restenting: Should we add a vest to the metal jacket? Catheter Cardiovasc Interv. 1999; 48:149–150. [PubMed: 10506768]
12. Messer RLW, Mickalonis J, Lewis JB, Omata Y, Davis CM, Brown Y, Wataha JC. Interactions between stainless steel, shear stress, and monocytes. J Biomed Mater Res A. 2007; 87:229–235. [PubMed: 18092353]
13. Kasprzak KS, Sunderman FW Jr, Salnikow K. Nickel carcinogenesis. Mutat Res. 2003; 533:67–97. [PubMed: 14643413]
14. Waksman R, Rajbabu P, Kuchulakanti PK, Baffour R, Hellinga D, Seabron R, Tio FO, Wittchow E, Hartwig S, Harder C, Rohde R, Heublein B, Andreae A, Waldmann K-H, Haverich A. Safety and efficacy of bioabsorbable magnesium alloy stents in porcine coronary arteries. Catheter Cardiovasc Interv. 2006; 68:607–617. [PubMed: 16969879]
15. Wu SK, Chu CL, Lin HC. Ion nitriding of equiatomic TiNi shape memory alloys II. Corrosion properties and wear characteristics. Surf Coat Technol. 1997; 92:206–211.
16. Villermaux F, Tabrizian M, Yahia L' H, Meunier M, Piron DL. Excimer laser treatment of NiTi shape memory alloy biomaterials. Appl Surf Sci. 1997; 110:109, 62–66.
17. Sella C, Martin JC, Lecoeur, Le Chanu A, Harmand MF, Naji A, Davidas JP. Biocompatibility and corrosion resistance in biological media of hard ceramic coatings sputter deposited on metal implants. Mater Sci Eng A. 1991; 139:49–57.
18. Lewis AL, Tolhurst LA, Stratford PW. Analysis of a phosphorylcholine-based polymer coating on a coronary artery stent pre- and post-implantation. Biomaterials. 2002; 23:1697–1706. [PubMed: 11922473]
19. Lahann J, Klee D, Thelen H, Bienert H, Vorwerk D, Höcker H. Improvement of haemocompatibility of metallic stents by polymer coating. J Mater Sci Mater Med. 1999; 10:443–448. [PubMed: 15348131]
20. Vom Dahl J, Haager PK, Grube E, Gross M, Beythien C, Kromer EP, Cattelaens N, Hamm CW, Hoffmann R, Reineke T, Klues HG. Effects of gold coating of coronary stents on neointimal proliferation following stent implantation. Am J Cardiol. 2002; 89:801–805. [PubMed: 11909562]
21. Hara H, Nakamura M, Palmaz JC, Schwartz RS. Role of stent design and coatings on restenosis and thrombosis. Adv Drug Deliv Rev. 2006; 58:377–386. [PubMed: 16650911]
22. Wieneke H, Sawitowski T, Wnendt S, Fischer A, Dirsch O, Karoussos IA, Erbel R. Stent coating: A new approach in interventional cardiology. Herz. 2005; 27:531–533.
23. Hasebe T, Shimada A, Suzuki T, Matsuoka Y, Saito T, Yohena S, Kamijo A, Shiraga N, Higuchi M, Kimura K, Yoshimura H, Kuribayashi S. Fluorinated diamond-like carbon as antithrombogenic coating for blood-contacting devices. J Biomed Mater Res A. 2005; 76:86–94. [PubMed: 16138324]
24. Heublein B, Özbek C, Pethig K. Silicon carbide-coated stents: Clinical experience in coronary lesions with increased thrombotic risk. J Endovasc Surg. 1998; 5:32–41. [PubMed: 9497204]
25. Unverdorben M, Sattler K, Degenhardt R, Fries R, Abt B, Wagner E, Koehler H, Scholz M, Ibrahim H, Tews K-H, Hennen B, Daemgen G, Berthold HK, Vallbracht C. Comparison of a silicon carbide coated stent versus a noncoated stent in humans: The TenaxTM-versus Nir TM-Stent Study (TENISS). J Interv Cardiol. 2003; 16:325–333. [PubMed: 14562673]
26. Harder C, Rzany A, Schaldach M. Coating of vascular stents with antithrombogenic amorphous silicon carbide. Prog Biomed Res. 1999; 4:71–77.
27. Hehrlein C. Stent passivation with silicon carbide as a possible alternative to drug-eluting stents—A comprehensive review of preclinical and clinical results. Interv Cardiol. 2009; 4:60–63.

28. Chu PK, Chen JY, Wang LP, Huang N. Plasma-surface modification of biomaterials. Mater Sci Eng. 2002; R 36:143–206.
29. Barranco V, Thiemann P, Yasuda HK, Stratmann M, Grundmeier G. Spectroscopic and electrochemical characterisation of thin cathodic plasma polymer films on iron. Appl Surf Sci. 2004; 229:87–96.
30. Liu CL, Chu PK, Lin GQ, Qi M. Anti-corrosion characteristics of nitride-coated AISI 316L stainless steel coronary stents. Surf Coat Technol. 2006; 201:2802–2806.
31. Xie D, Wan GJ, Maitz MF, Sun H, Huang N. Deformation and corrosion behaviors of Ti-O film deposited 316L stainless steel by plasma immersion ion implantation and deposition. Surf Coat Technol. 2013; 214:117–123.
32. Gomathi N, Rajasekar R, Babu RR, Mishra D, Neogi S. Development of bio/blood compatible polypropylene through low pressure nitrogen plasma surface modification. Mater Sci Eng C. 2012; 32:1767–1778.
33. Kim ES, Yu QS, Deng BL. Plasma surface modification of nanofiltration (NF) thin-film composite (TFC) membranes to improve anti organic fouling. Appl Surf Sci. 2011; 257:9863–9871.
34. Chen M, Hsieh TT, Osaki S, Zamora PO, Tsang R. Improvement of surface lubricity of polymers and metals by a glow-discharge plasma cross-linking process. J Biomater Sci. 2009; 20:511–527.
35. Starosvetsky D, Gotman I. Corrosion behavior of titanium nitride coated Ni-Ti shape memory surgical alloy. Biomaterials. 2001; 22:1853–1859. [PubMed: 11396890]
36. Chen M, Yu QS, Reddy CM, Yasuda HK. Model study investigating the role of interfacial factors in electrochemical impedance spectroscopy measurements. Corrosion. 2000; 56:709–721.
37. Maguire PD, McLaughlin JA, Okpalugo TIT, Lemoine P, Papakonstantinou P, McAdams ET, Needham M, Ogwu AA, Ball M, Abbas GA. Mechanical stability, corrosion performance and bioresponse of amorphous diamond-like carbon for medical stents and guidewires. Diamond Relat Mater. 2005; 14:1277–1288.
38. Lee SH, Kim JG, Choi HW, Lee KR. Microtensile strain on the corrosion performance of diamond-like carbon coating. J Biomed Mater Res A. 2008; 85:808–814. [PubMed: 17896779]
39. Gettens RTT, Gilbert JL. The electrochemical impedance of polarized 316L stainless steel: Structure–property-adsorption correlation. J Biomed Mater Res A. 2009; 90:121–132. [PubMed: 18491379]
40. Gonzalez JEG, Santana FJH, Mirza-rosca JC. Effect of bacterial biofilm on 316 SS corrosion in natural seawater by EIS. Corros Sci. 1998; 40:2141–2154.
41. Nagarajan S, Rajendran N. Surface characterisation and electro-chemical behaviour of porous titanium dioxide coated 316L stainless steel for orthopaedic applications. Appl Surf Sci. 2009; 255:3927–3932.
42. Hodgson AWE, Muller Y, Forster D, Virtanen S. Electrochemical characterisation of passive films on Ti alloys under simulated biological conditions. Electrochim Acta. 2002; 47:1913–1923.
43. Kartsonakis IA, Balaskas AC, Koumoulos EP, Charitidis CA, Kordas GC. Incorporation of ceramic nanocontainers into epoxy coatings for the corrosion protection of hot dip galvanized steel. Corros Sci. 2012; 57:30–41.
44. Thu QL, Bierwagen GP, Touzain S. EIS and ENM measurements for three different organic coatings on aluminum. Prog Org Coat. 2001; 42:179–187.
45. Wallinder D, Pan J, Leygraf C, Delblanc-Bauer A. EIS and XPS study of surface modification of 316LVM stainless steel after passivation. Corros Sci. 1998; 41:275–289.
46. Part 5: Tests for Cytotoxicity: In Vitro Methods. International Organization for Standardization; Geneva, Switzerland: 1999. 10993-5: Biological Evaluation of Medical Devices..

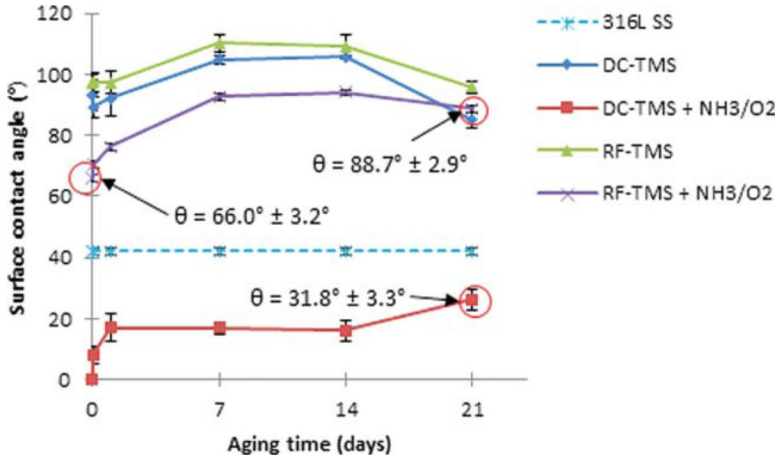

FIGURE 1.

Surface contact angle measurements of plasma coating deposited onto 316L stainless steel (SS) wafers. 316L SS, uncoated stainless steel; DC-TMS: TMS plasma coating using DC power supply; DC-TMS + NH_3/O_2: TMS plasma coating followed by additional NH_3/O_2 plasma surface modification using DC power supply; RF-TMS: TMS plasma coating using RF power supply; and RF-TMS + NH_3/O_2: TMS plasma coating followed by additional NH_3/O_2 plasma surface modification using RF power supply. [Color figure can be viewed in the online issue, which is available at wileyonlinelibrary.com.]

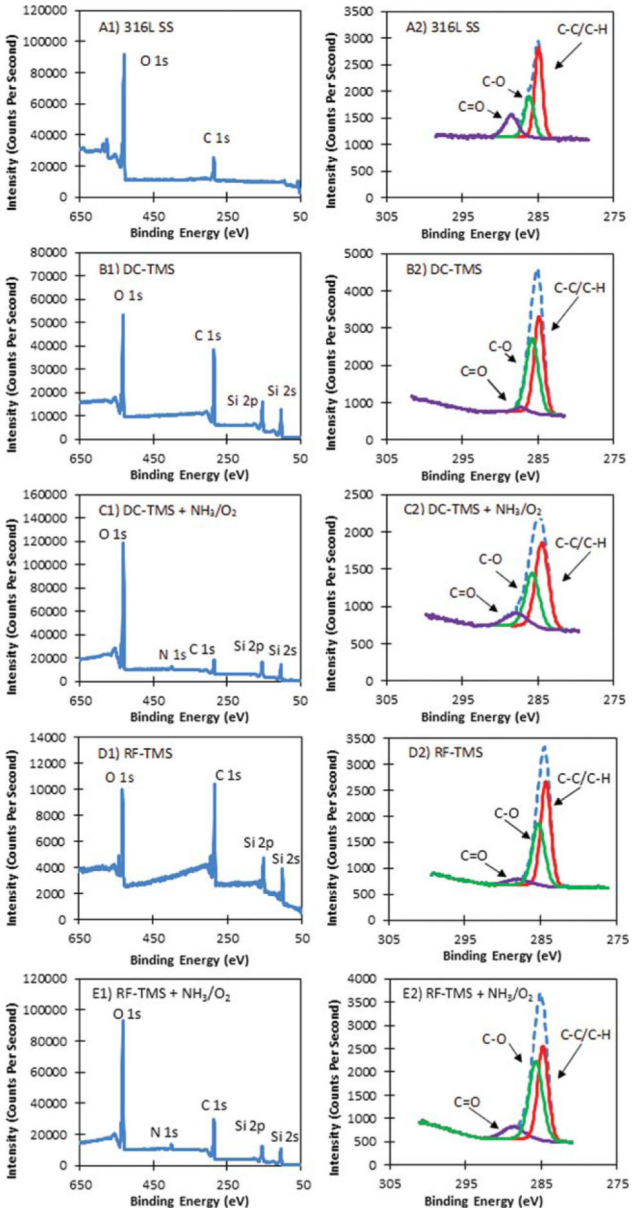

FIGURE 2.

XPS survey spectra A1 to E1 and high resolution deconvolutions of the C 1s peaks A2 to E2 for (A) 316L SS uncoated stainless steel, (B) DC-TMS plasma coating, (C) DC-TMS + NH_3/O_2 plasma coating, (D) RF-TMS plasma coating, and (E) RF-TMS + NH_3/O_2 plasma coating. [Color figure can be viewed in the online issue, which is available at wileyonlinelibrary.com.]

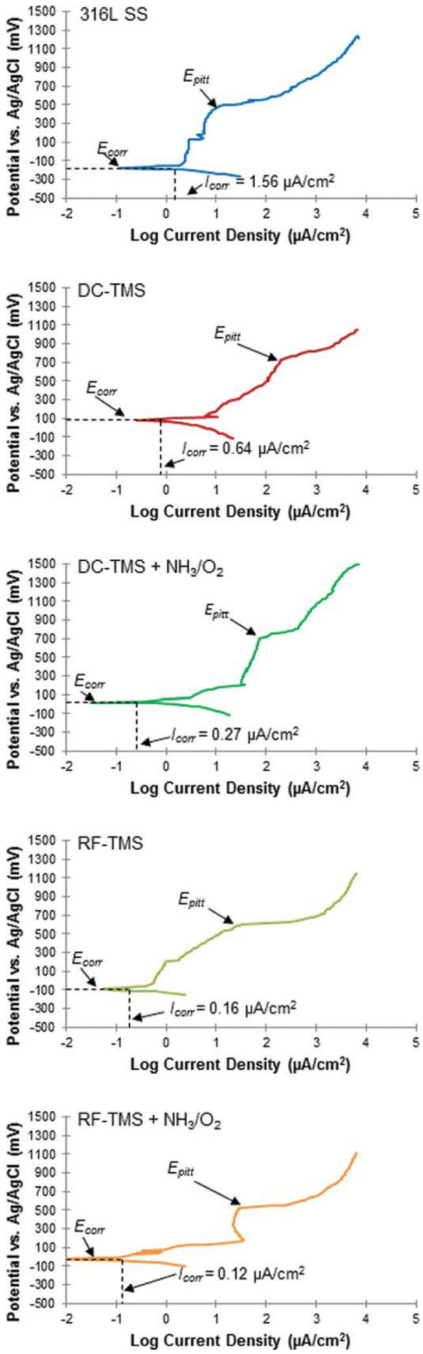

FIGURE 3.

Representative potentiodynamic polarization curves generated for as-deposited hydrophobic coating and surface-modified hydrophilic coating. [Color figure can be viewed in the online issue, which is available at wileyonlinelibrary.com.]

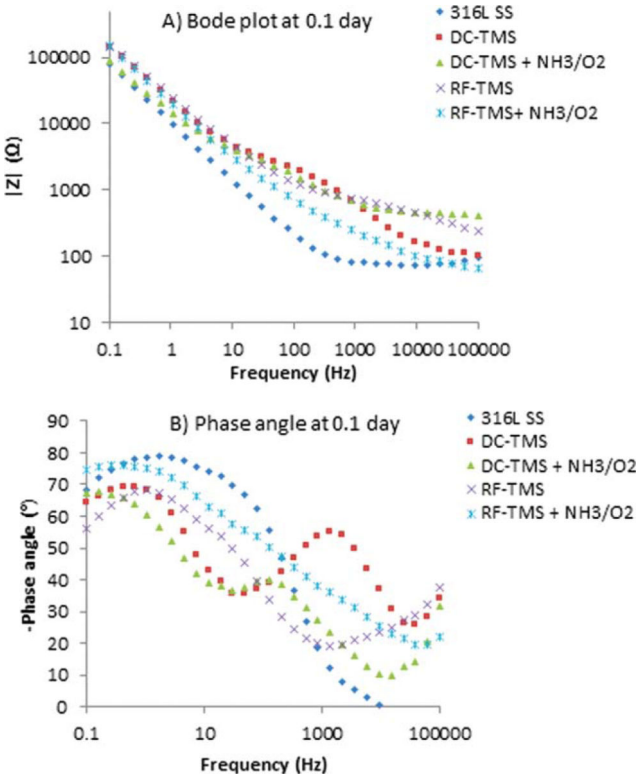

FIGURE 4.

Representative (A) Bode plots and (B) phase angle plots for stents after 0.1 day immersion in PBS. [Color figure can be viewed in the online issue, which is available at wileyonlinelibrary.com.]

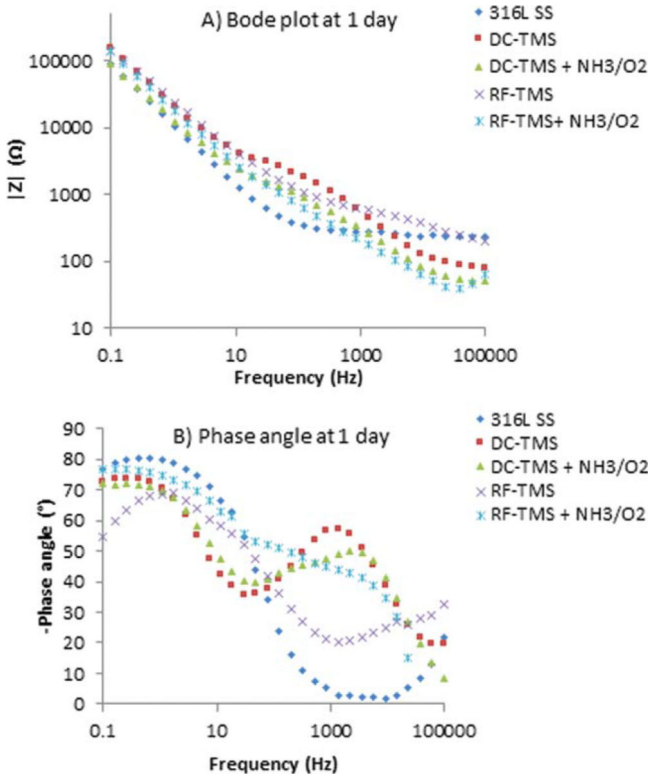

FIGURE 5.

Representative (A) Bode plots and (B) phase angle plots for stents after 1 day immersion in PBS. [Color figure can be viewed in the online issue, which is available at wileyonlinelibrary.com.]

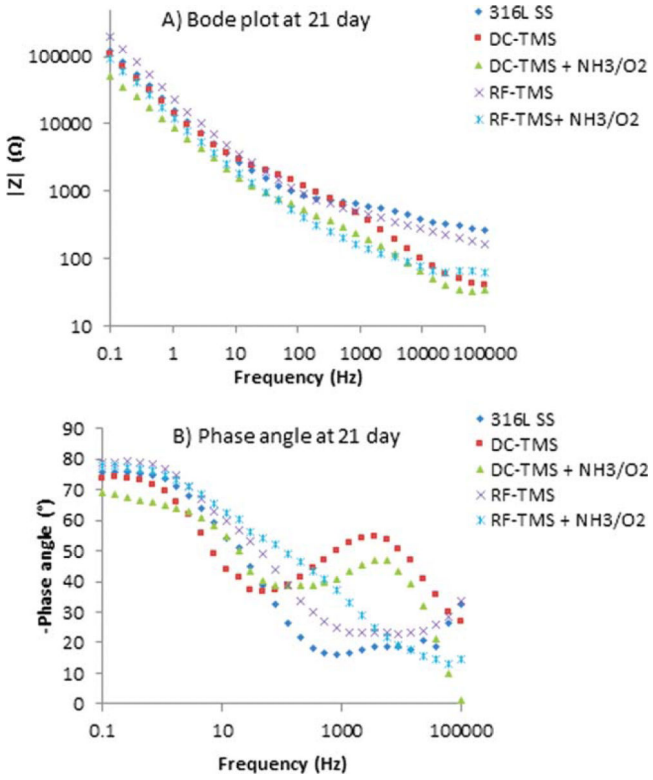

FIGURE 6.

Representative (A) Bode plots and (B) phase angle plots for stents after 21 day immersion in PBS. [Color figure can be viewed in the online issue, which is available at wileyonlinelibrary.com.]

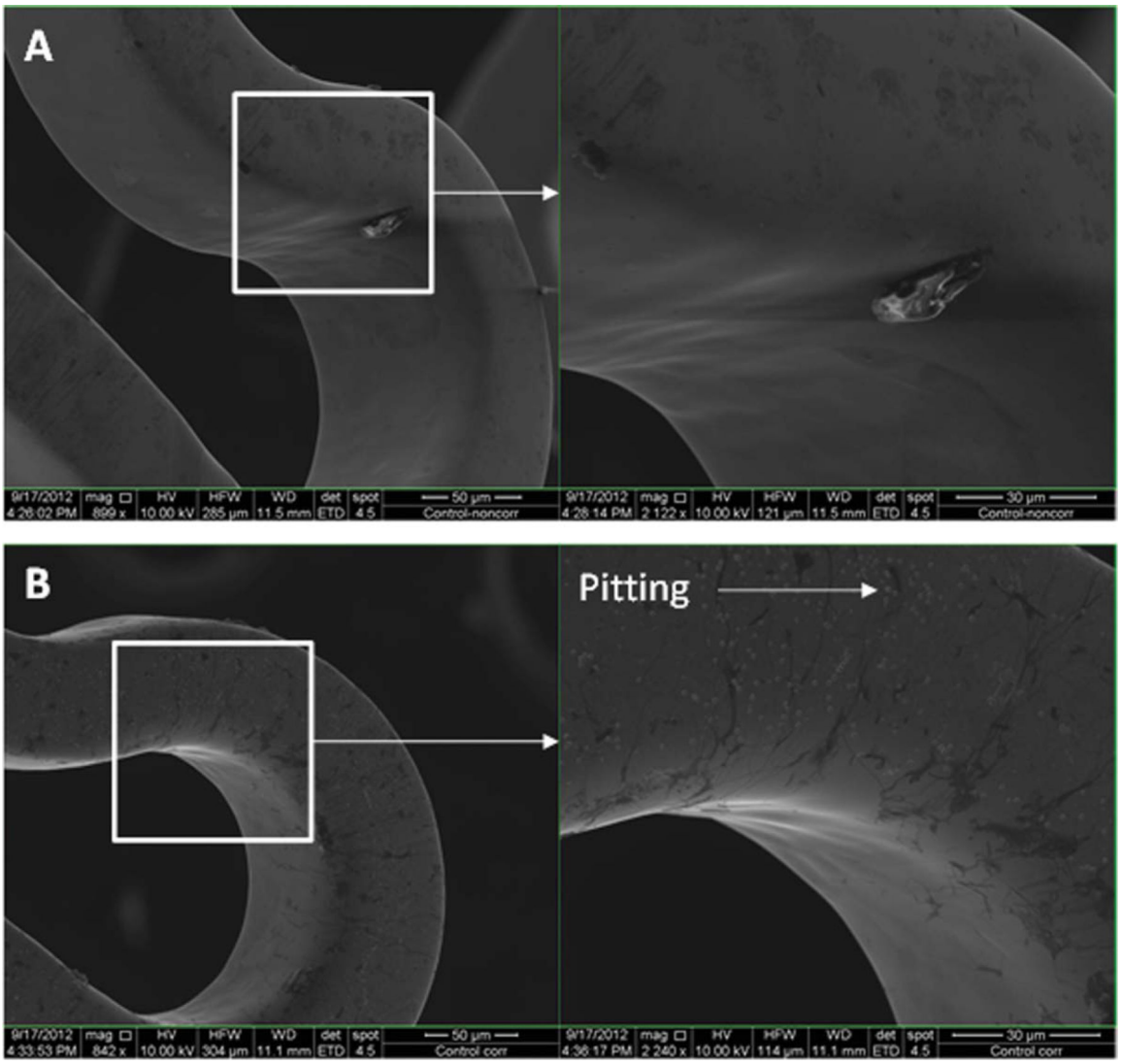

FIGURE 7.

SEM images of uncoated 316L stainless steel (SS) stents before (A) and after (B) potentiodynamic polarization testing. [Color figure can be viewed in the online issue, which is available at wileyonlinelibrary.com.]

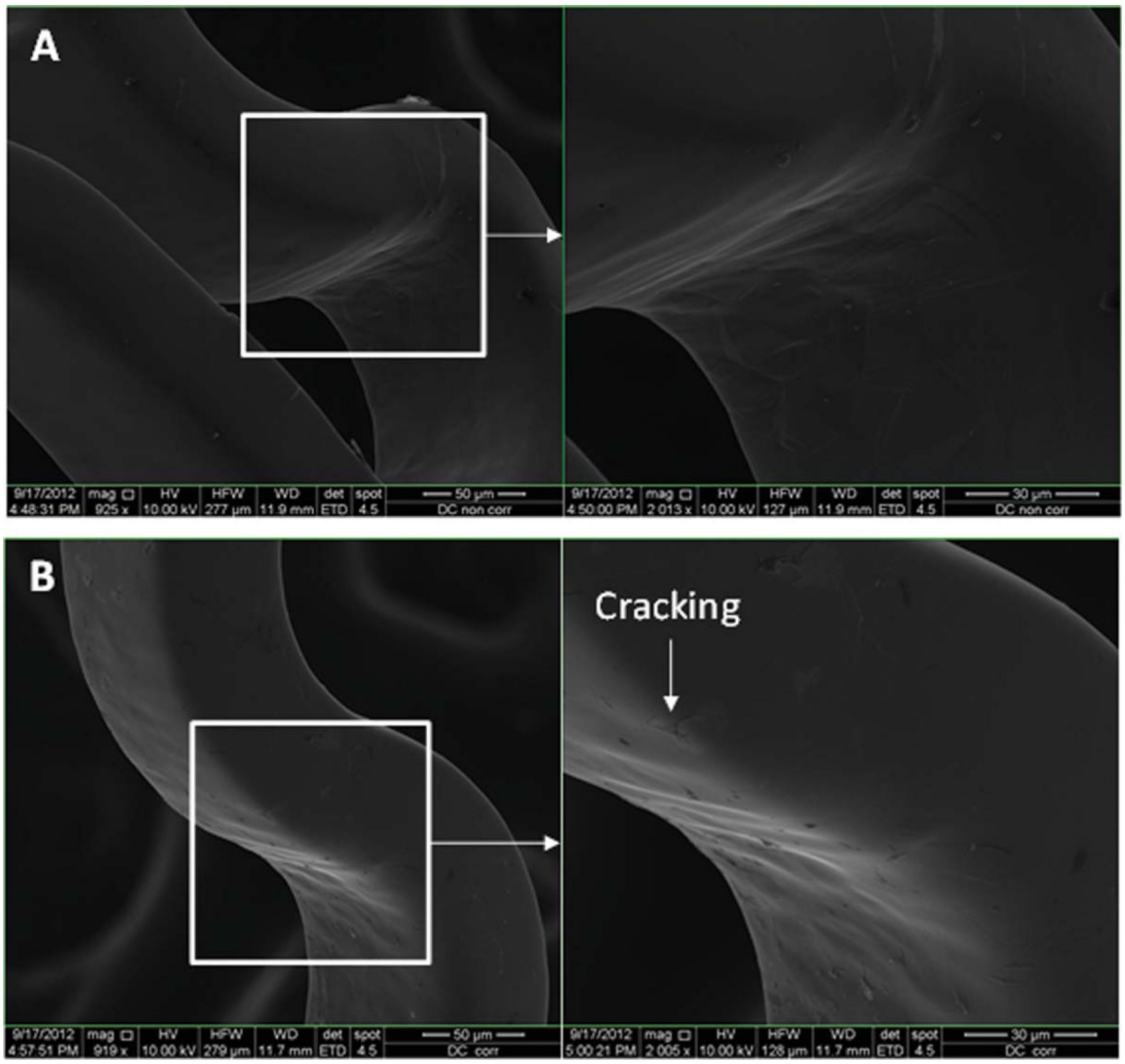

FIGURE 8.

SEM images of DC-TMS coated stents before (A) and after (B) potentiodynamic polarization testing. [Color figure can be viewed in the online issue, which is available at wileyonlinelibrary.com.]

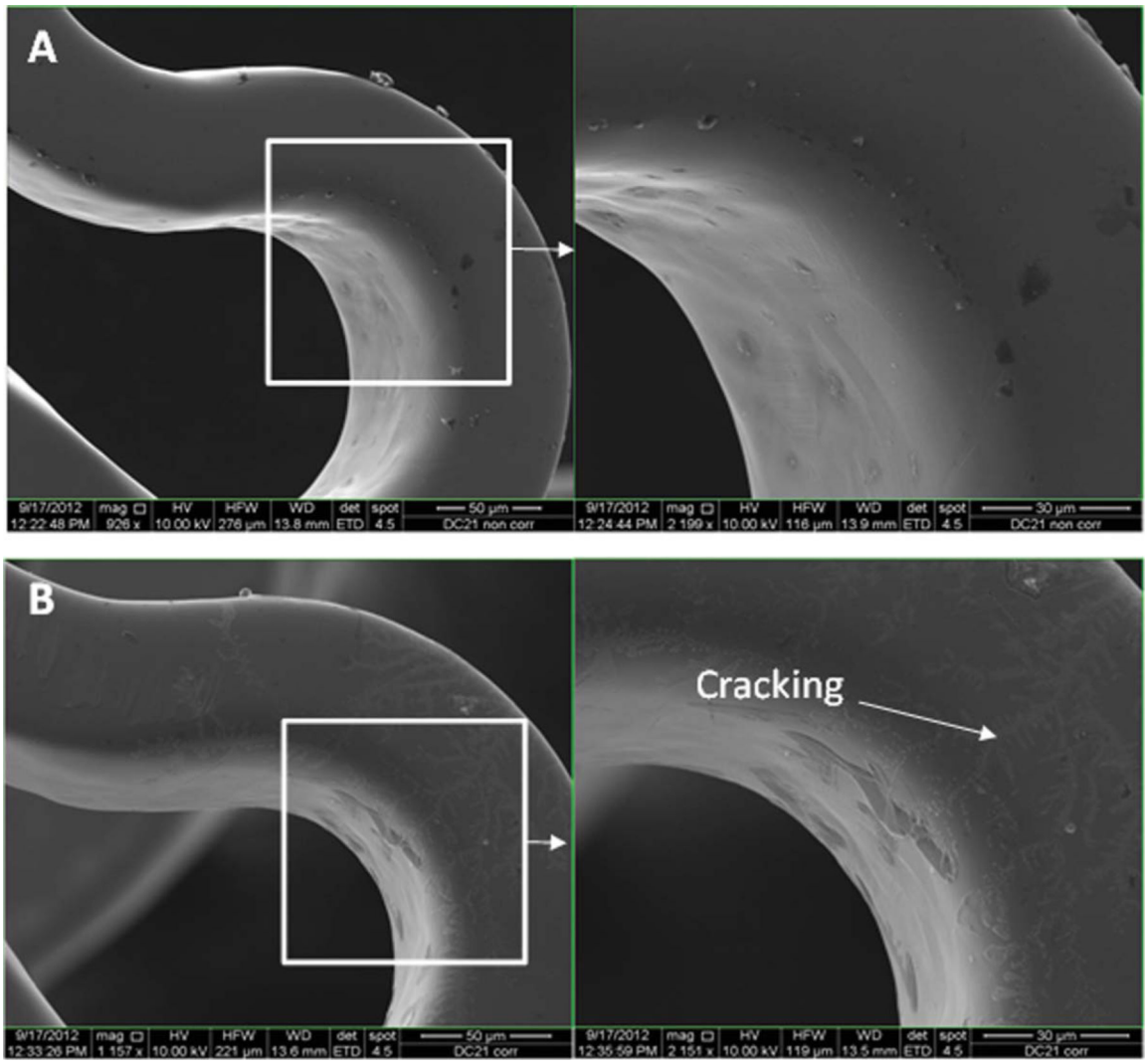

FIGURE 9.

SEM images of DC-TMS + NH_3/O_2 coated stents before (A) and after (B) potentiodynamic polarization testing. [Color figure can be viewed in the online issue, which is available at wileyonlinelibrary.com.]

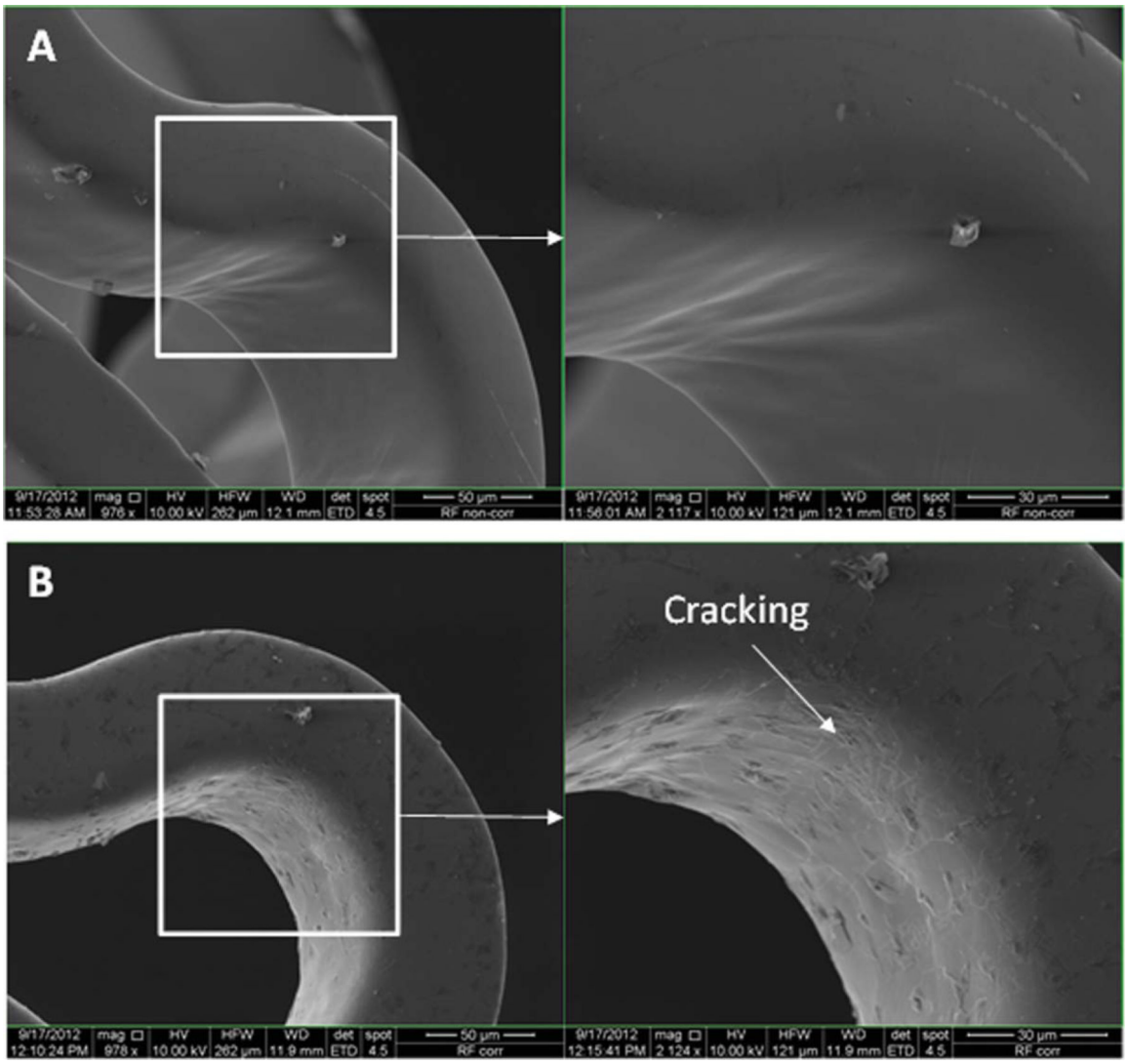

FIGURE 10.

SEM images of RF-TMS coated stents before (A) and after (B) potentiodynamic polarization testing. [Color figure can be viewed in the online issue, which is available at wileyonlinelibrary.com.]

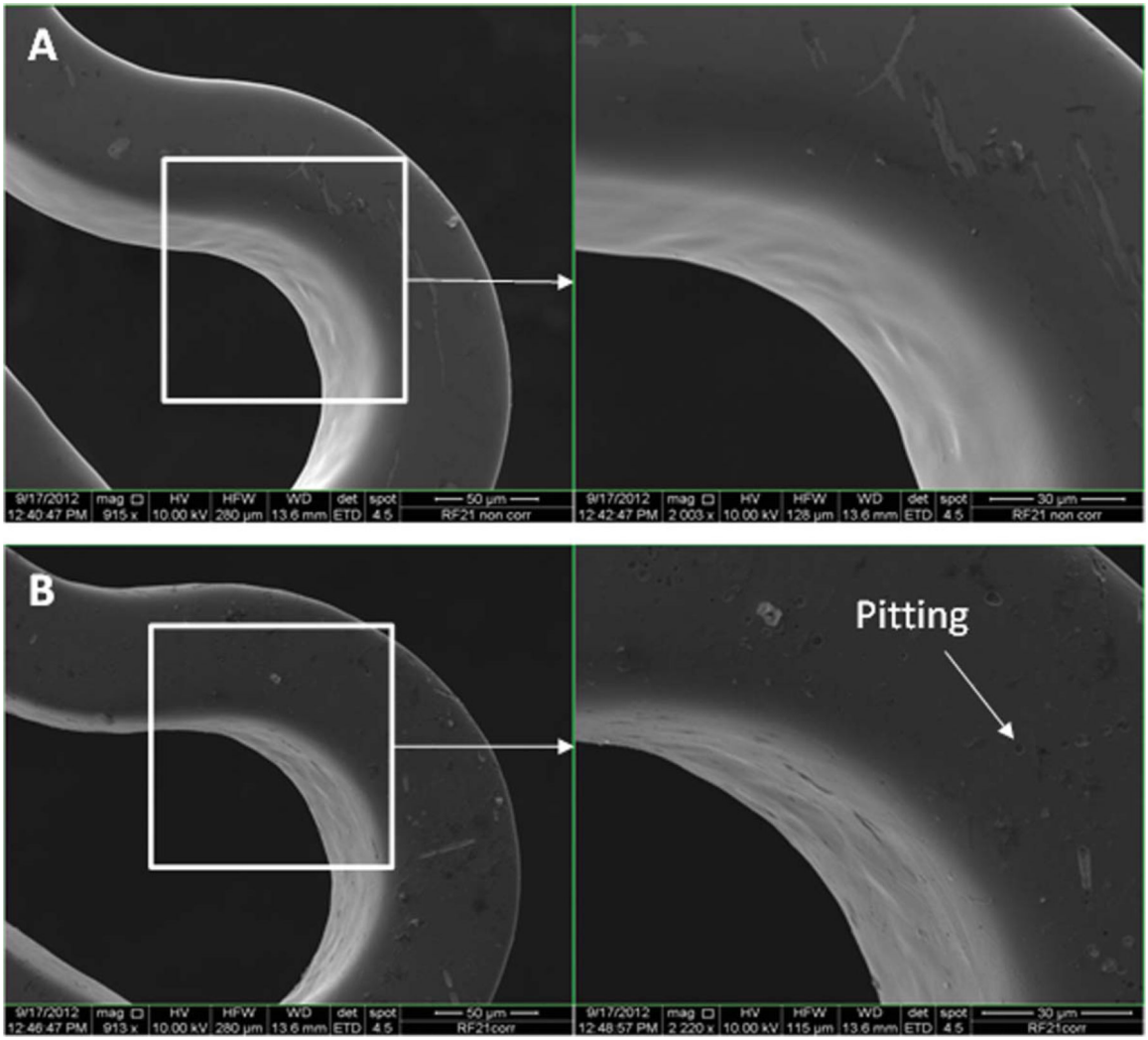

FIGURE 11.

SEM images of RF-TMS + NH_3/O_2 coated stents before (A) and after (B) potentiodynamic polarization testing. [Color figure can be viewed in the online issue, which is available at wileyonlinelibrary.com.]

TABLE I

Surface Elemental Composition of Stainless Steel as Determined by XPS Survey Scan (atomic %)

Sample ID	C	N	Si	O	Fe	Cr	Ni	Zn	Ti	Ca	Mo
316L SS	24.04	0.00	0.24	50.60	19.76	3.95	0.66	0.30	0.15	0.09	0.22
DC-TMS	53.14	0.00	23.02	23.84	0.00	0.00	0.00	0.00	0.00	0.00	0.00
DC-TMS + NH_3/O_2	21.36	2.86	18.78	55.19	0.23	0.00	0.00	0.00	0.00	0.00	0.00
RF-TMS	56.33	0.00	24.88	18.70	0.09	0.00	0.00	0.00	0.00	0.00	0.00
RF-TMS + NH_3/O_2	39.46	2.79	17.50	40.25	0.00	0.00	0.00	0.00	0.00	0.00	0.00

J Biomed Mater Res B Appl Biomater. Author manuscript; available in PMC 2015 September 04.

TABLE II

E_{corr}, Icorr and E_{pitt} Readings Determined from Potentiodynamic Polarization Curves for Plasma Coatings Deposited onto 316L Stainless Steel Stents in PBS Electrolyte with Ag/AgCl Reference Electrode

Treatment	E_{corr} (mV)	I_{corr} (μA/cm^2)	E_{pitt} (mV)
316L SS	–198.72 ± 22.53	4.09 ± 2.39	+461.4 ± 43.1
DC-TMS	+76.95 ± 6.93*	0.63 ± 0.10	+693.3 ± 27.7*
DC-TMS + NH_3/O_2	+9.88 ± 34.37*	2.54 ± 1.99	+710.6 ± 9.4*
RF-TMS	–64.58 ± 51.08*	0.16 ± 0.05	+612.0 ± 17.4*
RF-TMS + NH_3/O_2	–14.87 ± 50.60*	0.12 ± 0.08	+562.0 ± 67.6*

The data are presented as means 6 standard deviations for $n = 3$.

*(denotes $p < 0.05$, as compared to 316L SS).